The 7th International Supercritical $CO_2$ Power Cycles Symposium
February 21 – 24, 2022, San Antonio, Texas
Paper # 167

# Impact of selective admixture of additives to carbon dioxide on the size of $sCO_2$ power cycle key components

Sebastian Rath*
Institute of Power Engineering
TU Dresden
Dresden, Germany

Uwe Gampe
Institute of Power Engineering
TU Dresden
Dresden, Germany

Cornelia Breitkopf
Institute of Power Engineering
TU Dresden
Dresden, Germany

Andreas Jäger
Institute of Power Engineering
TU Dresden
Dresden, Germany

## ABSTRACT

High thermal efficiencies, smaller components, and a reduced overall plant footprint makes power cycles based on supercritical carbon dioxide ($sCO_2$) to one of the most promising candidates for the next generation of thermal energy systems. The critical temperature close to common ambient conditions combined with the high thermal stability of $CO_2$ enables a wide applicability for various heat sources of both conventional and regenerative origin.

Recent studies have shown that it is possible to further improve the performance of $sCO_2$-based power cycles by admixing of suitable additives. This is particularly of interest for situations where recooling to near-critical properties is challenging, such as solar thermal applications, or where lowering the critical point is intended to cool the process down to even lower temperatures without reaching the two-phase region. However, it has also been found that different additives can lead to a significant change in the enthalpy differences of the process, which may affect components sizes and functionality.

To address this issue, this work examines the impact of selected additives on key component sizes of $sCO_2$ power cycles. For this purpose, size correlations were developed, which enable a relative comparison of the component sizes for different $sCO_2$ blends. Fluid properties were calculated by using an innovative combination of mixture models, recently developed at our institute, supplemented with a correlation for transport properties. By applying our proposed methodology, corresponding changes in component sizes have been evaluated and are discussed for a selection of mixture candidates and different $sCO_2$ cycle architectures.

## INTRODUCTION

Due to several advantages, like higher thermal efficiencies or a reduction in size and complexity of single components, power cycles with supercritical $CO_2$ as working medium are considered as a promising replacement for conventional processes for various heat sources of both

*Corresponding author, sebastian.rath@tu-dresden.de

conventional and regenerative origin [1–4]. However, because these advantages are essentially linked to the critical point, which for $CO_2$ is located at 7.377 MPa and 304.128 K (30.98°C) [5], this virtually results in a limitation of the process parameters. Additionally, due to strong variations of fluid properties near the critical point, even small changes in the recooling conditions can cause large deviations in efficiency, which is especially challenging for applications at elevated temperatures such as concentrated solar power (CSP). In this context, various studies have shown that one option could be the admixture of suitable additives, which on the one hand shift the critical point to higher temperatures at which recooling to ambient can be achieved more easily, and which on the other hand may lead to even higher thermal efficiencies of the cycle [6–9]. However, in a previous study [6] we showed that different additives can lead to a significant change in the enthalpy differences of the process, which may affect components sizes, functionality and cost predictions. While cost correlations of individual components are usually based on the overall performance or, in the case of heat exchangers, on the heat exchanger conductance and the heat exchanger surface ($U \cdot A$) [10,11], a direct comparison of sizes is of particular interest when it comes to the selection of designs, e.g. the type of a turbomachine or a preliminary estimate of suitability of existing components to be used with mixtures or an impure medium. Up to now, studies on the effect of the admixture of additives to $CO_2$ on the component size can be found only rarely and are mostly associated with cost analyses [9,12].

In this context Valencia-Chapi et al. [9] conducted a comprehensive study on the influence of different binary mixtures for use in line-focused solar power plants. Size considerations were involved indirectly as part of a cost estimation. For the heat exchangers a fixed product of the heat exchanger conductivity and the exchanger surface ($U \cdot A$) is set to evaluate the amount of transferred heat with changing mixtures influencing the thermal efficiency. Vesely et al. [12] studied the influence of impurities on several components. Additions of He, CO, $O_2$, $N_2$ $H_2$, $CH_4$ and $H_2S$ were investigated separately as binary mixtures for two different cycle architectures. In this context approximate changes in the heat transfer coefficient and the associated channel lengths of the heat exchangers were investigated. However, a detailed description of the method and boundary conditions used for the analysis as well as for the mixing models used to predict fluid properties is not provided.

## BASIC MODELING APPROACH AND BOUNDARY CONDITIONS

For fluid modeling, a predictive combination of a multi-fluid mixture model with excess Gibbs energy models ($g^E$-models) was used. This approach, which was recently developed by our group, allows the usage of the best available equation of state for each pure substance, such as the reference equation of state for $CO_2$ by Span and Wagner [5], together with the best available predictive model, such as the $g^E$-models UNIFAC [13] or COSMO-SAC [14–16]. A more detailed description of these models can be found in previous work [17,18].

Transport properties were calculated using a generalized multi-parameter correlation by Chung et al. [19]. This method requires only few input variables and is applicable for polar and nonpolar fluids. In a comparison with other methods by Tilly et al. [20], the correlation showed a good agreement with experimental values of several supercritical $CO_2$ mixtures.

Implementation of the fluid properties into the calculation model was done using the thermo-physical property software TREND 4.0 [21] supplemented by a set of custom extensions written in Python.

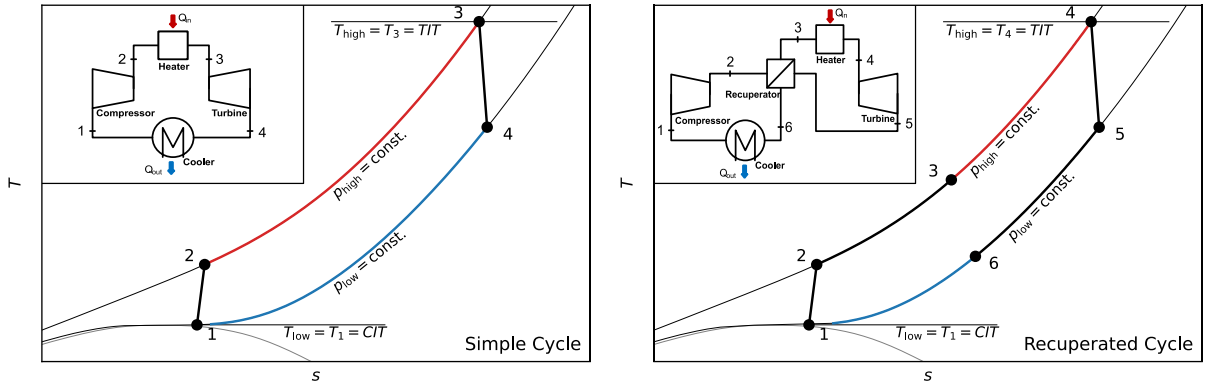

Figure 1: Block diagrams and T-s diagrams of the considered cycle architectures

## CYCLE ARCHITECTURES AND BOUNDARY CONDITIONS

For evaluation two rather simple cycle architectures were chosen, which have also been used for a comprehensive fluid screening in our previous work [6]. As shown in the left part of Figure 1 the first layout consists of a simple cycle including only the essential main components. Starting at process point ,1 the fluid is compressed in a compressor to the upper pressure level at point 2. From point 2, heat is added in an isobaric heater to reach the upper temperature level of the cycle at point 3, which corresponds to the turbine inlet temperature (TIT). After expansion in a turbine back to the lower pressure level in point 4, excess heat is rejected in an isobaric recooler until the compressor inlet temperature (CIT) is reached back in point 1. For the second layout, as shown on the right hand side of Figure 1, the simple cycle is extended by a recuperator. By this means, part of the heat at the turbine outlet in point 5 can be transferred back to the compressed fluid from the compressor outlet in point 2. The recuperation was modeled by setting a minimum pinch point difference $\Delta T_{\mathrm{R}}$ at the cold end of the recuperator, i.e. $T_6 = T_2 + \Delta T_{\mathrm{R}}$. Additionally, all heat exchangers were calculated by splitting them up in a finite number of steps including a check for possible phase changes, multiphase flows or pinch point violations. For the comparison of both cycles, the thermal efficiency was used, which can be calculated by

$$\eta_{\mathrm{th,SC}} = 1 - \frac{h_4 - h_1}{h_3 - h_2} \tag{1}$$

for the simple cycle and by

$$\eta_{\mathrm{th,RC}} = 1 - \frac{h_6 - h_1}{h_4 - h_3} \tag{2}$$

for the recuperated cycle.

The boundary conditions applied on the cycles are listed in Table 1 and were oriented on a parameter range typical for waste heat applications with possible air-recooling to elevated ambient conditions. Thus, the minimum temperature, representing the temperature at the compressor inlet (CIT), is set to an elevated temperature level of 40 °C while the upper temperature has been fixed at 500 °C, which corresponds to the turbine inlet temperature (TIT). Pressure levels were set to a near critical value of 7.4 MPa for the lower pressure level and 20 MPa for the upper pressure level. Losses were treated in terms of isentropic efficiencies for the compressor and the turbine. For the recuperator, a minimum pinch point difference of 10 K was applied. Pressure losses were neglected.

Table 1: Boundary conditions applied to both cycles

| Boundary condition | Symbol | Value |
|---|---|---|
| Minimum temperature | $\vartheta_{\mathrm{low}} \equiv \mathrm{CIT}$ | 40 °C |
| Maximum temperature | $\vartheta_{\mathrm{high}} \equiv \mathrm{TIT}$ | 500 °C |
| Lower pressure level | $p_{\mathrm{low}}$ | 7.4 MPa |
| Upper pressure level | $p_{\mathrm{high}}$ | 20 MPa |
| Compressor efficiency | $\eta_{\mathrm{C}}$ | 0.8 |
| Turbine efficiency | $\eta_{\mathrm{T}}$ | 0.9 |
| Min. pinch point difference recuperator | $\Delta T_{\mathrm{R}}$ | 10 K |
| Admixture fraction | x | 0 - 0.2 |

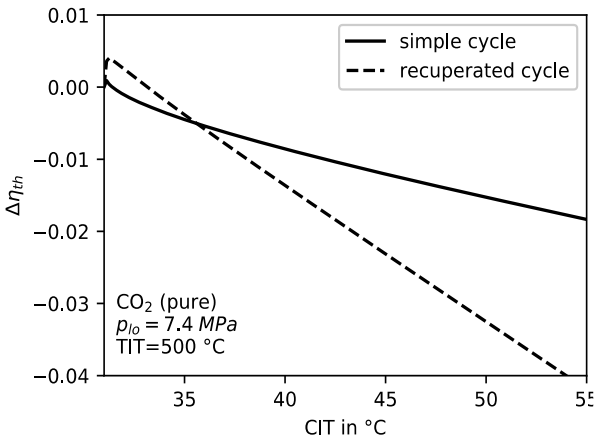


Figure 2: Change in thermal efficiency with increasing compressor inlet temperature (CIT) for both cycles operated with pure $CO_2$

Regarding these boundary conditions, starting near the critical point at 31°C, Figure 2 shows the absolute change in efficiency for both cycles with increasing compressor inlet temperatures, representing operation at higher ambient conditions. As can be seen in the graph, despite a small increase at the beginning, the efficiency drops significantly for both cycles with higher temperatures. At a compressor inlet temperature of 40 °C the thermal efficiency has dropped by 0.005 for the simple and about 0.015 for the recuperated cycle, decreasing further with higher temperatures. The aforementioned small increases are caused by the pseudo-critical point at the chosen inlet pressure of 7.4 MPa, which is slightly higher than the critical pressure $p_{\mathrm{crit}} = 7.3773$ MPa [22].

To compare the influences of admixtures on the component sizes the four mixture candidates $H_2S$ (hydrogen sulfide), $C_3H_8$ (propane) and the two noble gases Kr (krypton) and Xe (xenon) have been chosen. For each of these fluids, when added to an $sCO_2$ cycle operated at elevated ambient conditions, higher thermal efficiencies compared to the use of pure $CO_2$ could be demonstrated in past studies. In this context, Valencia-Chapi et al. [9] reported efficiency increases up to 3 % by adding $H_2S$ or $C_3H_8$ to an $sCO_2$-recompression cycle operated at elevated inlet temperatures. Similar increases could be noted by addition of Kr and Xe in a comprehensive screening in our previous work [6]. Regarding the boundary conditions used in this work, Figure 3 compares the influence of admixtures on the thermal efficiency of both cycle architectures with increasing CIT by adding various fractions of the selected additives. Breaks or interruptions in these lines indicate that the composition has led to a critical point higher than the individual inlet

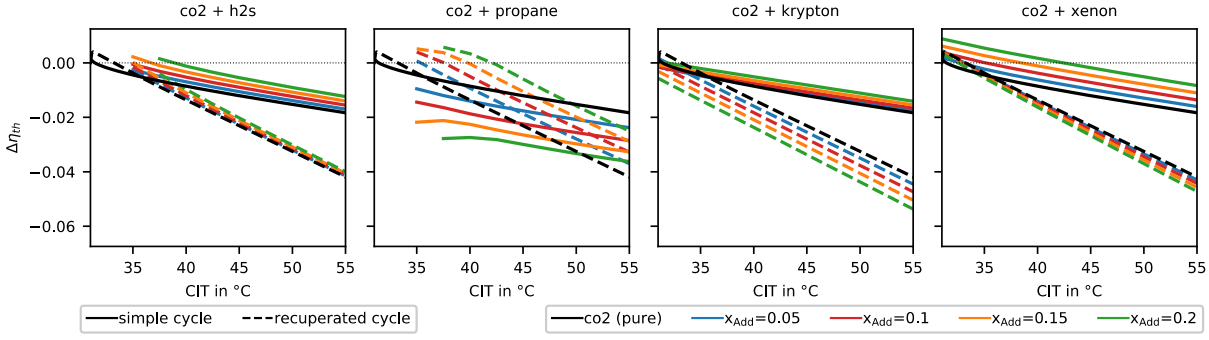


Figure 3: Effect of admixture of the selected additives to both cycles operated at elevated inlet conditions

conditions or that multiple phases are present at least at one point of the cycle. Since only single-phase, supercritical mixtures have been considered, these results were discarded and are therefore not shown in the graphs. Starting from the left of Figure 3, it can be seen that the addition of $H_2S$ leads to higher thermal efficiencies especially in the simple cycle increasing with higher fractions of the admixture. The offset in the beginning of the lines at lower temperatures also suggests, with increasing amount of additive, a shift of the critical point to higher temperatures. The addition of propane shows increases in thermal efficiency for the recuperated cycle but on the other hand large decreases for the simple cycle architecture, with, again, stronger impact for higher concentrations. As for the previous mixture of $H_2S$ and $CO_2$, the discontinuity of the lines for lower temperatures shows a shift of the critical point, which had also been demonstrated in previous work [6]. As can be seen in the two last plots, the two noble gases show a somewhat similar behavior leading to higher efficiencies for the simple cycle but a reverse effect for the recuperated case. However, while significant increases, even above the reference value for $CO_2$ at 31°C, are already noticeable with smaller amounts of Xe, only minor improvements can be found by adding Kr up concentrations of $x$ =0.2. More significant improvements of the thermal efficiency are expected with higher admixtures, which, however, are not addressed within the scope of this study.

With reference to the previously mentioned mixture modeling the admixture of $H_2S$, $C_3H_8$, and Kr was modeled using the reference equations of state [23,24] in combination with adjusted mixing parameters. Since no adapted parameters were available for $CO_2$+Xe, the reference equation of state [23] in combination with the $g^E$-model COSMO-SAC was used for fluid properties.

## COMPONENT SIZE CORRELATIONS

The individual size of real components depends on a variety of design parameters, which are not directly related to the fluid composition itself and can be varied within limits during the design process. These parameters include, for example, the construction type, the shape of the flow-conducting components or the choice of materials. In order to get a comparability between individual mixtures, it is thus assumed that the components, excluding the turbomachinery, always rely on the same design. This requires also, that key parameters which are not directly connected to the fluid properties, are treated as fixed and identical for all cases. Within these boundaries size factors can be derived which are solely related to process- and fluid properties allowing a relative estimate of the size of the components for different operating media.

Neglecting secondary parts such as flanges, baffles or framing components, the volume of the heat exchangers is considered to result from the flow cross-section required to handle a given mass-flow of fluid as well as the length needed for heat transfer. The cross-section can be directly related to the mass flow $\dot{m}$, the average flow velocity $\bar{c}$ (perpendicular to the flow cross-section) and the average density $\bar{\rho}$:

$$A_{sq} = \frac{\dot{m}}{\bar{c} \cdot \bar{\rho}} \tag{3}$$

With the previously made assumptions of constant design parameters ($\bar{c} = \text{const.}$), this can be reduced to a simple factor which depends only on the mass flow and the average density:

$$f_{A,HX} = \dot{m} \cdot (\bar{\rho})^{-1} \tag{4}$$

Assuming that the heat source remains the same for all mixtures a relational value for the mass

flow can be formed from the reciprocal of the fluids enthalpy difference in the heater (index $H$):

$$\dot{m} = \frac{\dot{Q}_{\mathrm{H}}}{\Delta h_{\mathrm{H}}} = \frac{1}{\Delta h_{\mathrm{H}}} \mid \dot{Q}_{\mathrm{H}} \overset{\text{def}}{=} \dot{Q}_{\mathrm{H,CO2}} \overset{\text{def}}{=} \dot{Q}_{\mathrm{H,Mix}} \overset{\text{def}}{=} \dot{Q} \overset{\text{def}}{=} \text{const.} \tag{5}$$

Based on the process architectures described previously, without flow splits or taps, this value is taken as constant for all the other components.

To derive a length factor, the general heat transfer equation is assumed:

$$\dot{Q} = \Delta h \cdot \dot{m} = \bar{\alpha} \cdot A_{\mathrm{surf}} \cdot \Delta T = \bar{\alpha} \cdot \pi \cdot d \cdot L \cdot \Delta T \tag{6}$$

In which $\bar{\alpha}$ denotes the mean heat transfer coefficient, $d$ the wetted diameter of the channel, $L$ the channel length and $\Delta T$ the (logarithmic) mean temperature difference. Assuming the wetted diameter to be the channel diameter, rearranging to $L$ and substituting $\bar{\alpha}$ with its definition for pipe flow ($Nu \cdot \frac{\lambda}{d}$) yields:

$$L = \frac{\Delta h \cdot \dot{m}}{\bar{\lambda} \cdot Nu \cdot \pi \cdot \Delta T} \tag{7}$$

Now, Eq. ((7) can be further expanded using the well-known McAdams form of the Dittus-Boelter-correlation as described by Winterton [25] for turbulent flow in smooth circular pipes,

$$Nu = 0.023 \cdot Re^{0.8} \cdot Pr^{n} \text{ with } \begin{cases} n = 0.3 \mid T_{\mathrm{fluid}} > T_{\mathrm{wall}} \\ n = 0.4 \mid T_{\mathrm{fluid}} \leq T_{\mathrm{wall}} \end{cases} \tag{8}$$

and subsequently the appropriate definitions for the Reynolds-number ($Re = c \cdot d_{\mathrm{h}} \cdot \rho / \eta$) and the Prandtl-number ($Pr = \eta \cdot c_p / \lambda$) can be used to obtain:

$$L = \frac{\Delta h \cdot \dot{m}}{\lambda \cdot 0.023 \cdot Re^{0.8} \cdot Pr^{n} \cdot \pi \cdot \Delta T} = \frac{\Delta h \cdot \dot{m} \cdot \left(\frac{\bar{c}_p \cdot \bar{\eta}}{\bar{\lambda}}\right)^{-n}}{0.023 \cdot \pi \cdot \Delta T \cdot \bar{\lambda} \cdot \left(\frac{c \cdot d_{\mathrm{h}} \cdot \bar{\rho}}{\bar{\eta}}\right)^{0.8}} \tag{9}$$

After eliminating all constants ($c, d_{\mathrm{h}}, 0.023, \pi$), a relative comparison factor is obtained equivalent to the cross-section, which is only dependent on the mean fluid properties and process variables:

$$f_{L,HX} = \frac{\Delta h \cdot \dot{m} \cdot \left(\frac{\bar{c}_p \cdot \bar{\eta}}{\bar{\lambda}}\right)^{-n}}{\Delta T \cdot \bar{\lambda} \cdot \left(\frac{\bar{\rho}}{\bar{\eta}}\right)^{0.8}} \tag{10}$$

Again, the mass-flow is given by Equation (5). However, since no secondary media are specified for the heater or the recooler, $\Delta T$ is taken as constant for these two components in a simplified manner. For the recuperator, the mean temperature difference, which has been obtained within the stepwise calculation of both sides, has been used.
Finally, the relative factor for the heat exchanger volume is obtained from base area and length:

$$f_{V,HX} = f_{A,HX} \cdot f_{L,HX} \tag{11}$$

The size of turbomachinery depends essentially on its construction type, which in turn is directly linked to fluid and operating parameters. Assuming a single-stage machine, its design is determined by selecting two independent design values. Typically, this is done using dimensionless parameters of which, in this case, the specific speed and the specific diameter, denoted by $\sigma$ and $\delta$, were used. The former is given by the following relation,

$$\sigma = n \cdot \frac{2 \cdot \sqrt{\pi \cdot \dot{V}}}{(2 \cdot \Delta h)^{3/4}} = n \cdot \frac{2 \cdot \sqrt{\pi \cdot \frac{\dot{m}}{\rho}}}{(2 \cdot \Delta h)^{3/4}} \tag{12}$$

in which $n$ denotes the rotational speed to be chosen within the design procedure, $\rho$ corresponds to the inlet fluid density and $\Delta h$ to the enthalpy difference assuming an isentropic compression. Taking $n$ as constant, the expression can be reduced in a way equivalent to the procedure for heat exchangers and thus, a formulation depending only on process- and fluid parameters can be obtained:

$$\sigma^* = \frac{\sqrt{\dot{m}/\rho}}{\Delta h^{3/4}} \tag{13}$$

As before, the mass flow is given by Equation (5) as a relation of the enthalpy difference to the density. As a second parameter, the characteristic diameter contains the size information in the form of the impeller diameter $D$:

$$\delta = \frac{D}{\sqrt{\frac{4 \cdot \dot{V}}{\pi \cdot \sqrt{2 \cdot \Delta h}}}} = \frac{D}{\sqrt{\frac{4 \cdot \dot{m}/\rho}{\pi \cdot \sqrt{2 \cdot \Delta h}}}} \tag{14}$$

However, a functional design with a good efficiency is linked to an appropriate combination of both parameters. In this context, a suitable relation can be found within specific speed / diameter charts (Cordier diagram) providing a range of favorable combinations. For usage within this work, a functional relation of both parameters is obtained by fitting curves along the line of highest efficiencies for selected data points. The data was taken from a chart provided by Bohl and Elmendorf [26]. The result of the fit can be seen in Figure 4, giving the following relations:

$$\delta_C = \ln(3.715 \cdot \sigma^{-0.141}) + 0.297 \cdot \sigma^{-1.422} \tag{15}$$

for compressors and

$$\delta_T = ln(3.173 \cdot \sigma^{-0.285}) + 0.182 \cdot \sigma^{-1.293} \tag{16}$$

for turbines. However, it can be assumed that the reduced form of $\sigma$ from Equation (13), compared to its original formulation in Equation (12), leads to rather untypical values for the specific speed which are probably outside the range covered by the charts. To prevent extrapolation errors when applying the fits, the ratio of the specific speeds can be related to a reference value:

$$\sigma_{\mathrm{MIX,i}} = \sigma_{\mathrm{CO2,Ref,i}} \cdot \frac{{\sigma^*}_{\mathrm{MIX,i}}}{{\sigma^*}_{\mathrm{CO2,i}}} \tag{17}$$

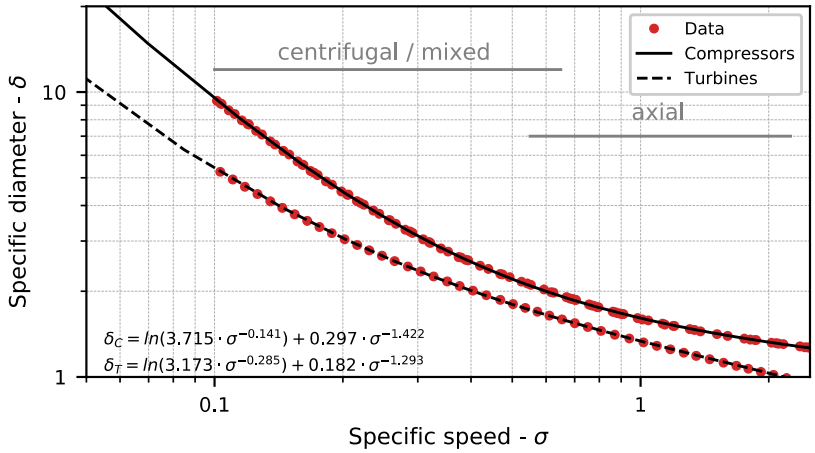

Figure 4: Fitted Cordier lines for compressors and turbines

Here, $i$ denotes either the compressor or the turbine. At least one value for $\sigma_{\mathrm{CO2,Ref,i}}$ has to be selected freely within the Cordier diagram (cf. Figure 4) according to the type of construction to set as default. The second value is either also chosen directly from the diagram or determined by assuming the same rotational speed and taking the relational factors from Equation (13:

$$\sigma_{\mathrm{CO2,Ref,T}} = \sigma_{\mathrm{CO2,Ref,C}} \cdot \frac{\sigma^*_{CO2,T}}{\sigma^*_{CO2,C}} \tag{18}$$

Within this work, a value of $\sigma_{\mathrm{CO2,Ref,C}} = 0.5$ was set for the compressor, which was then used to calculate the value for the turbine by means of Equation (18). Finally, the specific diameters $\delta$ can be calculated using either Equation (15) or Equation (16) for the compressor or the turbine respectively.

## RESULTS AND DISCUSSION

Calculations were done for various amounts of the selected fluids up to molar fractions of $x$ = 0.2, to be compared to a operation with pure $CO_2$ at the boundary conditions specified in Table 1 for each cycle architecture. Results are compiled in Figure 5, showing effects on the shape and location of the process in the $h$-$s$ diagram as well as changes in the enthalpy differences and the relative size factors for the individual components (compressor, turbine, recooler, recuperator, heater) in both cycle architectures. Referring to this, the subscripts “sim” (≙ simple) and “rec” (≙ recuperated) show the relation of the components to the respective cycle architecture. If these designations are missing, the components were treated as identical for both cycles. Additionally, Figure 6 shows the relative changes in the specific speed and the specific diameter of the turbomachines in the Cordier diagram.

Beginning with the uppermost row in Figure 5, it can be seen that also for higher fractions of $H_2S$ in $CO_2$, only slight differences can be noticed in the $h$-$s$ diagram. There is a slightly weaker slope of both isobars as well as a distinct reduction in the compressors enthalpy difference, which is also evident in the bar-plot, shown in Figure 5b. By adding a fraction of $x$ = 0.2 of $H_2S$ to $CO_2$ (green bars) the enthalpy difference in the compressor $\Delta h_{\mathrm{C}}$ can be reduced by over 10 % compared to the use of pure $CO_2$. In contrast, the enthalpy difference in the turbine $\Delta h_{\mathrm{T}}$ remains nearly unaffected in all cases.

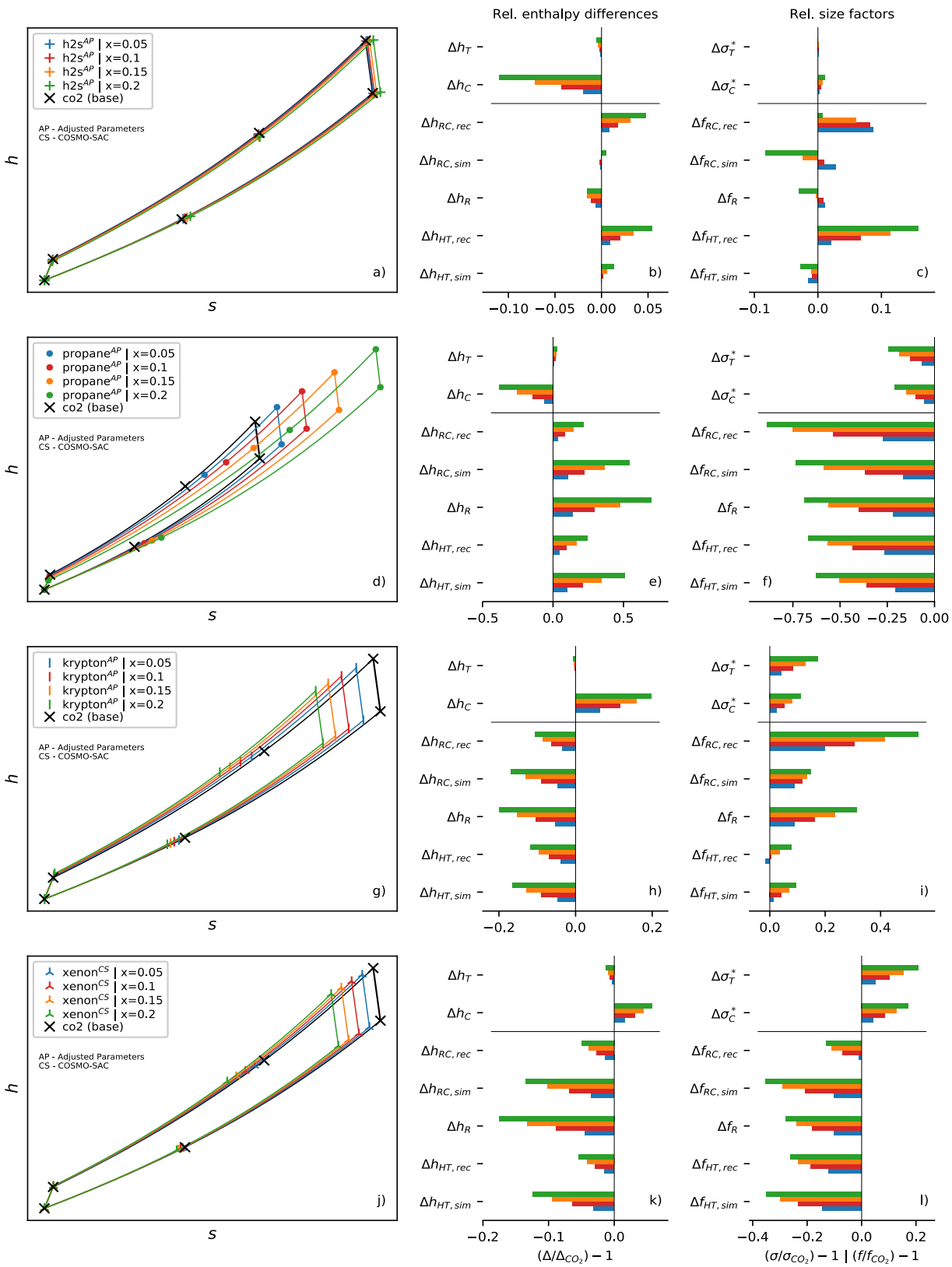


Figure 5: Effects of the selected additives on the shape and location of the process in the *h*-*s* diagram, the differences in the enthalpies in the single components for both cycle architectures and the relative influence on the component sizes when compared to the use of pure $CO_2$

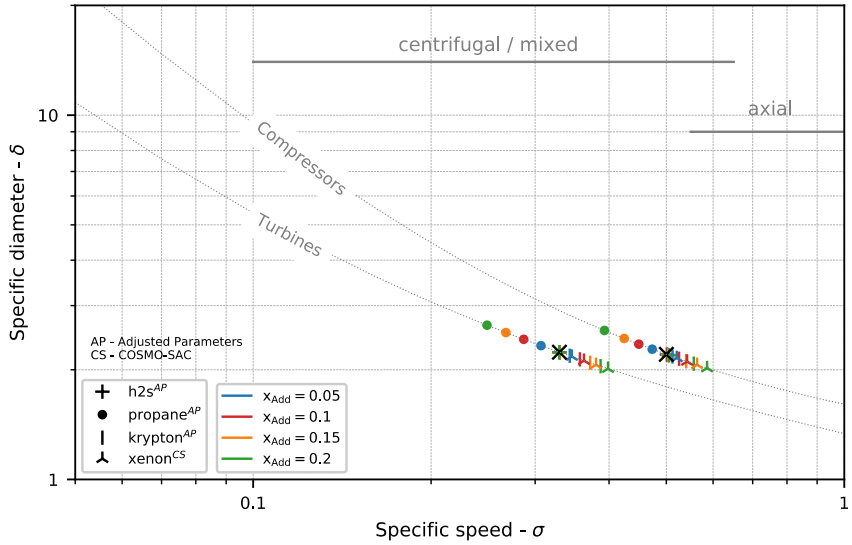


Figure 6: Effects of the selected admixtures on the specific values for the compressor and the turbine in the Cordier diagram

Regarding the heat exchangers of the simple cycle, denoted by the subscript “sim”, also here the enthalpy differences show only minor changes. Noticeable is a reversal of effects regarding the recooler. While the enthalpy difference $\Delta h_{\mathrm{RC,sim}}$ decreases for small quantities of $H_2S$, it increases again for $x$ = 0.15 and higher. However, the changes are hardly noticeable. When recuperation is considered, a significantly stronger impact on the relative enthalpy difference in the heat exchangers ($\Delta h_{\mathrm{RC,rec}}$, $\Delta h_{\mathrm{R}}$, $\Delta h_{\mathrm{HT,rec}}$) can be noticed with increasing amount of $H_2S$. While there is a decrease in the enthalpy difference in the recuperator $\Delta h_R$ with increasing admixture, the situation is different for the heater $\Delta h_{\mathrm{HT,rec}}$ and the recooler $\Delta h_{\mathrm{RC,rec}}$, where up to approximately 5 % more heat must be added or dissipated at $x$ = 0.2, shown by the green bars in Figure 5b.

With reference to the relative changes in size, calculated by the correlations presented in this work, the bar plot in Figure 5c show that for the compressor ($\Delta\sigma_{\mathrm{C}}{}^{*}$), despite the aforementioned reduction in the enthalpy difference $\Delta h_{\mathrm{C}}$, there is only a slight trend to higher specific speeds with higher admixtures. For the turbine ($\Delta\sigma_{\mathrm{T}}{}^{*}$), equivalently to the change in the enthalpy difference there is hardly any visible difference. Including the specific diameters, also the position in the Cordier diagram in Figure 6 remains nearly unaffected. Thus, an almost identical machine size, compared to the use of pure $CO_2$, can be assumed. However, for the heat exchangers in both cycles, the relative sizes of the recoolers $\Delta f_{\mathrm{RC,sim}}$ and $\Delta f_{\mathrm{RC,rec}}$ show an opposite behavior regarding the changes in the enthalpy differences described before. While the latter increase in both cases with increasing amounts of $H_2S$, the relative sizes decrease starting from a positive initial value and changing to negative values for mole fractions of $H_2S$ higher than $x$ = 0.15, indicating smaller components with regard to the use of pure $CO_2$. The same can be noticed for the difference in the size factor of the recuperator $\Delta f_{\mathrm{R}}$, which changes from a positive to a negative relative value for fractions higher than $x$ = 0.15. Finally, although both heaters, for the simple cycle as well for the recuperated cycle, show increasing values for the enthalpy differences $\Delta h_{\mathrm{HT,sim}}$ and $\Delta h_{\mathrm{HT,rec}}$, with increasing content of $H_2S$, different trends can be observed for their relative changes in size. While in the recuperated case $\Delta f_{\mathrm{HT,rec}}$ increases with the concentration of $H_2S$, it decreases for the simple cycle ($\Delta f_{\mathrm{HT,sim}}$) and, moreover, shows an non-monotonic behavior, indicating an unbalanced change in the fluid properties with changing content of $H_2S$.

When looking at propane in Figure 5d, the shapes of the $h$-$s$ diagram show on the one hand a

trend of shifting the upper process level to higher values for $h$ and $s$ and on the other hand, a trend of lowering the compressor's enthalpy differences for higher fractions of propane. The same is also evident in the bar chart in Figure 5e when comparing the relative enthalpies. While the relative enthalpy difference in the turbine $\Delta h_{\mathrm{T}}$ remains almost unaffected, a significant reduction in the difference of the compression enthalpy $\Delta h_{\mathrm{C}}$ up to 0.5 can be seen with increasing amounts of propane in $CO_2$. At a mole fraction of $x$ = 0.2 (Figure 5e, green bar) the compression enthalpy is almost reduced by half compared to the use of pure $CO_2$. As a result of the trend to higher enthalpies of the upper process level, the enthalpy differences for all heat exchangers increase significantly for both cycles with increasing amounts of propane. When taking into account the relative changes in component sizes, see Figure 5f, the specific speed for both turbomachines is reduced by up to approx. 25 % at a mole fraction of propane of $x$ = 0.2. With regard to the positions in the Cordier diagram shown in Figure 6, this leads to higher specific diameters and thus to a potential increase in size. In contrast, despite increasing enthalpy differences, all heat exchangers show a significant decrease in relative volume with increasing fractions of propane. The highest impact can be noted for the recooler in the recuperated cycle architecture ($\Delta f_{\mathrm{RC,rec}}$). Its size is reduced by more than 75 % at a fraction of $x$ = 0.2 of propane. This is remarkable since this reduction is achieved despite increasing enthalpy differences, indicating higher amounts of heat to be transferred. With regard to the size calculations in Equation (4) and Equation (10), a reason for this might be the specific heat capacity and the density which both for propane are significantly higher than for $CO_2$.

For the two noble gases krypton and xenon the $h$-$s$ diagrams in Figure 5g and Figure 5j show an slight increase in the slope of the isobars and a trend to lower enthalpy values with higher fractions of admixture, whereas both effects are somewhat more pronounced with krypton than with xenon. This is also evident in the bar plots in Figure 5h and Figure 5k, which show a distinct reduction in the relative enthalpy differences for all heat exchangers with increasing mole fractions of both fluids. While also the relative enthalpy difference in the turbines $\Delta h_{\mathrm{T}}$ tends to slightly lower values, a considerable increase in the enthalpy difference can be seen for the compressors ($\Delta h_{\mathrm{C}}$). It is noticeable that the relative increase in compressor enthalpy is lower for xenon than for krypton, which one of the main factors for the improved overall performance of the mixture in terms of efficiency (cf. Figure 3). Referring to the changes in the specific speeds $\Delta\sigma^*_{\mathrm{C}}$ and $\Delta\sigma^*_{T}$ both xenon and krypton show increased values for both machines, which, regarding the corresponding specific diameters in the Cordier diagram in Figure 6, lead to potential smaller component sizes. However, a completely different behavior can be seen in case of the relative size factors for the heat exchangers. For krypton for almost all heat exchangers a significant increase in the size can be noted. This is particularly evident in the recuperated case in which the relative size difference for the recooler $\Delta f_{\mathrm{RC,rec}}$ shows an increase of approximately 50 % compared to the use of pure $CO_2$. Only for the heater of the same cycle architecture, slight reductions in the difference of the size factor $\Delta f_{HT,\mathrm{rec}}$ can be seen for low fractions of krypton. For xenon the trend reverses. Instead of higher relative size values, a reduction in the relative size factors of the heat exchangers can be observed for all mole fractions. A connection to krypton is mainly apparent due to the fact that some components with a large change to higher values for krypton show smaller reductions in size for xenon compared to other components. This is particularly evident in case of the relative size factor differences for the recooler $\Delta f_{\mathrm{RC,rec}}$ and the recuperator $\Delta f_{\mathrm{R}}$.

## CONCLUSION

In this work, the impact of selective admixture of additives to supercritical carbon dioxide has been studied for a selection of four mixture candidates to be used as working fluids in two different thermodynamic cycles operated at elevated ambient conditions. For this, a set of size

correlations was derived by simplifying common design approaches to depend only on fluid and cycle specific properties. Based on the assumptions made, these correlations allowed a relative comparison of component sizes for different fluid mixtures with reference to the use of pure $CO_2$. As a result, depending on the mixture, changes in component sizes of more than 75 % have been found. Generally, it has been shown that sizes may vary significantly even at small amounts of additives and are not necessarily bound only to the enthalpy differences in the devices. In addition, it is apparent that component sizes may not follow a uniform trend with increasing mixture concentration which would have to be examined in more detail for individual cases. The same applies to the approaches for the size correlations for which the assumptions made to reduce the base equations to rely only on fluid properties may not cover all design cases. An example may be the Nusselt correlation used in Equation (8), which is valid only for turbulent flows.

Nevertheless, the approach can show that by using fluid mixtures, significant changes in component sizes can be expected even with small amounts of secondary media, underlining the potential of admixing additives to $sCO_2$. Adapted to the corresponding case and in particular with respect to the fluid-based optimization of $sCO_2$ cycles, the correlations proposed in this work allow the inclusion of approximate component sizes in the objective functions. Without the need of detailed information about the individual component designs this enables a more precise formulation of optimization targets even at early evaluation phases.
Future works will focus on the validation of the method, as well as the application to more complex cycle architectures and an enhanced selection of mixture candidates.

## REFERENCES


[1] Y. Ahn, S.J. Bae, M. Kim, S.K. Cho, S. Baik, J.I. Lee, J.E. Cha, Review of supercritical CO2 power cycle technology and current status of research and development, Nuclear Engineering and Technology. 47 (2015) 647–661. https://doi.org/10.1016/j.net.2015.06.009.

[2] U. Gampe, J. Henoch, G. Gerbeth, F. Hannemann, S. Rath, U. Hampel, S. Glos, Concept and preliminary design of a 600 °C+ sCO2 test facility, in: Proceedings of the 2nd European SCO2 Conference 2018, Essen, Germany, 2018. https://doi.org/10.17185/duepublico/46084.

[3] S. Glos, M. Wechsung, R. Wagner, A. Heidenhof, D. Schlehuber, Evaluation of sCO2 power cycles for direct and waste heat applications, (2018). https://doi.org/10.17185/DUEPUBLICO/46082.

[4] J. Yin, Q. Zheng, Z. Peng, X. Zhang, Review of supercritical $CO_2$ power cycles integrated with CSP, Int J Energy Res. 44 (2020) 1337–1369. https://doi.org/10.1002/er.4909.

[5] R. Span, W. Wagner, A New Equation of State for Carbon Dioxide Covering the Fluid Region from the Triple-Point Temperature to 1100 K at Pressures up to 800 MPa, J. Phys. Chem. Ref. Data. 25 (1996) 1509–1596. https://doi.org/10.1063/1.555991.

[6] S. Rath, E. Mickoleit, U. Gampe, C. Breitkopf, A. Jäger, Study of the influence of additives to CO2 on the performance parameters of a sCO2-cycle, Conference Proceedings of the European SCO2 Conference4th European SCO2 Conference for Energy Systems: March 23-24. 2021 (2021) 212. https://doi.org/10.17185/DUEPUBLICO/73965.

[7] S. Baik, J.I. Lee, Preliminary Study of Supercritical CO2 Mixed With Gases for Power Cycle in Warm Environments, (2018) 8.

[8] G. Manzolini, M. Binotti, D. Bonalumi, C. Invernizzi, P. Iora, CO2 mixtures as innovative working fluid in power cycles applied to solar plants. Techno-economic assessment, Solar Energy. 181 (2019) 530–544. https://doi.org/10.1016/j.solener.2019.01.015.

[9] R. Valencia-Chapi, L. Coco-Enríquez, J. Muñoz-Antón, Supercritical CO2 Mixtures for Advanced Brayton Power Cycles in Line-Focusing Solar Power Plants, Applied Sciences. 10 (2019) 55.

https://doi.org/10.3390/app10010055.

[10] N.T. Weiland, B.W. Lance, S.R. Pidaparti, sCO2 Power Cycle Component Cost Correlations From DOE Data Spanning Multiple Scales and Applications, in: Volume 9: Oil and Gas Applications; Supercritical CO2 Power Cycles; Wind Energy, American Society of Mechanical Engineers, Phoenix, Arizona, USA, 2019: p. V009T38A008. https://doi.org/10.1115/GT2019-90493.

[11] T. Drennen, B. Lance, An Integrated Techno-economic Modeling Tool for sCO2 Brayton Cycles, 2019. https://doi.org/10.2172/1762938.

[12] L. Vesely, K.R.V. Manikantachari, S. Vasu, J. Kapat, V. Dostal, S. Martin, Effect of Impurities on Compressor and Cooler in Supercritical CO2 Cycles, Journal of Energy Resources Technology. 141 (2019) 012003. https://doi.org/10.1115/1.4040581.

[13] A. Fredenslund, R.L. Jones, J.M. Prausnitz, Group-Contribution Estimation of Activity Coefficients in Nonideal Liquid Mixtures, AIChE J. 21 (1975) 1086–1099.

[14] S.-T. Lin, S.I. Sandler, A Priori Phase Equilibrium Prediction from a Segment Contribution Solvation Model, Ind. Eng. Chem. Res. 41 (2002) 899–913. https://doi.org/10.1021/ie001047w.

[15] S.-T. Lin, S.I. Sandler, A Priori Phase Equilibrium Prediction from a Segment Contribution Solvation Model. - Additions and Corrections, Ind. Eng. Chem. Res. 43 (2004) 1322–1322. https://doi.org/10.1021/ie0308689.

[16] C.-M. Hsieh, S.I. Sandler, S.-T. Lin, Improvements of COSMO-SAC for vapor–liquid and liquid–liquid equilibrium predictions, Fluid Phase Equilibria. 297 (2010) 90–97. https://doi.org/10.1016/j.fluid.2010.06.011.

[17] A. Jäger, I.H. Bell, C. Breitkopf, A theoretically based departure function for multi-fluid mixture models, Fluid Phase Equilib. 469 (2018) 56–69. https://doi.org/10.1016/j.fluid.2018.04.015.

[18] A. Jäger, E. Mickoleit, C. Breitkopf, A Combination of Multi-Fluid Mixture Models with COSMO-SAC, Fluid Phase Equilib. 476 (2018) 147–156. https://doi.org/10.1016/j.fluid.2018.08.004.

[19] T.H. Chung, M. Ajlan, L.L. Lee, K.E. Starling, Generalized multiparameter correlation for nonpolar and polar fluid transport properties, Ind. Eng. Chem. Res. 27 (1988) 671–679. https://doi.org/10.1021/ie00076a024.

[20] K.D. Tilly, N.R. Foster, S.J. Macnaughton, D.L. Tomasko, Viscosity correlations for binary supercritical fluids, Ind. Eng. Chem. Res. 33 (1994) 681–688. https://doi.org/10.1021/ie00027a028.

[21] R. Span, R. Beckmüller, T. Eckermann, S. Herrig, S. Hielscher, A. Jäger, E. Mickoleit, T. Neumann, S.M. Pohl, B. Semrau, M. Thol, TREND. Thermodynamic Reference and Engineering Data 4.0, Lehrstuhl fuer Thermodynamik, Ruhr-Universitaet Bochum, Bochum, Germany, 2019.

[22] K. Brun, P. Friedman, R. Dennis, Fundamentals and applications of supercritical carbon dioxide (sCO2) based power cycles, 1st edition, Elsevier, Waltham, MA, 2017.

[23] E.W. Lemmon, R. Span, Short Fundamental Equations of State for 20 Industrial Fluids, J. Chem. Eng. Data. 51 (2006) 785–850. https://doi.org/10.1021/je050186n.

[24] E.W. Lemmon, M.O. McLinden, W. Wagner, Thermodynamic Properties of Propane. III. A Reference Equation of State for Temperatures from the Melting Line to 650 K and Pressures up to 1000 MPa, J. Chem. Eng. Data. 54 (2009) 3141–3180. https://doi.org/10.1021/je900217v.

[25] R.H.S. Winterton, Where did the Dittus and Boelter equation come from?, International Journal of Heat and Mass Transfer. 41 (1998) 809–810. https://doi.org/10.1016/S0017-9310(97)00177-4.

[26] W. Bohl, W. Elmendorf, Strömungsmaschinen 1 - Aufbau und Wirkungsweise, 11th ed., Vogel Buchverlag, 2013.